sensitivity. Reproduction of the observed radiance record requires a global moistening of the upper troposphere in response to atmospheric warming that is roughly equivalent in magnitude to that predicted under the assumption of constant relative humidity. This behavior is consistent with that simulated from current models and provides key quantitative evidence in support of their ability to predict the climate feedback from upper tropospheric water vapor. Given the importance of water vapor feedback in determining the climatic response to anthropogenic forcings, such confirmation is essential to the use of these models for global warming projections.

References and Notes

1. J. Kiehl, K. Trenberth, *Bull. Am. Meteorol. Soc.* **78**, 197 (1997).
2. U. Cubasch, R. Cess, in *Climate Change: The IPCC Scientific Assessment*, J. T. Houghton *et al.*, Eds. (Cambridge Univ. Press, Cambridge, 1990).
3. R. Cess *et al.*, *J. Geophys. Res.* **95**, 16601 (1990).
4. A. Raval, V. Ramathan, *Nature* **342**, 758 (1989).
5. R. Pierrehumbert, *J. Atmos. Sci.* **52**, 1784 (1995).
6. D. Rind *et al.*, *Nature* **349**, 500 (1991).
7. A. Del Genio, W. Kovari, Y. Mao-Sung, *Geophys. Res. Lett.* **21**, 2701 (1994).
8. T. Stocker *et al.*, in *Climate Change 2001: Contribution of Working Group I to the Third Assessment Report of the Intergovernmental Panel on Climate Change* (Cambridge Univ. Press, Cambridge, 2001), pp. 418–470.
9. I. Held, B. Soden, *Annu. Rev. Energy Environ.* **25**, 441 (2000).
10. R. Colman, *Geophys. Res. Lett.* **31**, L21109 (2004).
11. R. Wetherald, S. Manabe, *J. Atmos. Sci.* **45**, 1397 (1988).
12. B. J. Soden, R. T. Wetherald, G. L. Stenchikov, A. Robock, *Science* **296**, 727 (2002).
13. R. Lindzen, *Bull. Am. Meteorol. Soc.* **71**, 288 (1990).
14. R. E. Dickinson *et al.*, in *Climate Change 1995: The Science of Climate Change*, J. T. Houghton *et al.*, Eds. (Cambridge Univ. Press, Cambridge, 1996), pp. 193–227.
15. D. Sun, R. Lindzen, *J. Atmos. Sci.* **50**, 1643 (1993).
16. R. Lindzen *et al.*, *Bull. Am. Meteorol. Soc.* **82**, 417 (2001).
17. K. Minschwaner, A. Dessler, *J. Clim.* **17**, 1272 (2004).
18. Under a constant relative humidity, the concentration of water vapor is determined by changes in the equilibrium vapor pressure, which increases rapidly with temperature. The Clausius-Clapeyron equation dictates that the fractional increase in equilibrium vapor pressure (e_s) scales according to $d(\ln e_s)/dT \sim 1/T^2$ (where T is absolute temperature). Near the surface, this would lead to roughly a 6% increase in water vapor mass per 1 K warming. In the upper troposphere, where temperatures are colder, the water vapor mass increases at roughly twice this rate (*9*).
19. The water vapor mixing ratio (w) is defined as the mass of water vapor per unit mass of dry air. The relative humidity (r) is determined as the ratio of the water vapor mixing ratio to its "saturated" or equilibrium value (w_s), expressed in percent; $r = 100 \times w/w_s$. The total column water vapor (W) is defined as the vertically integrated mass of water vapor per unit area in units of kg/m^2; $W = \int w\rho\, dz$, where ρ is the density of air and z is altitude, and the integration is performed from the surface to the top of the atmosphere.
20. Model simulations are from the GFDL atmospheric GCM integrated with observed ocean SSTs; see (*41*) for a description of the atmospheric model and SST data set.
21. See supporting data on *Science* Online.
22. R. Ross, W. Elliott, *J. Clim.* **14**, 1602 (2001).
23. P. Zhai, R. Eskridge, *J. Clim.* **10**, 2643 (1997).
24. K. Trenberth, J. Fasullo, L. Smith, *Clim. Dyn.* **24**, 741 (2005).
25. F. Wentz, M. Schabel, *Nature* **403**, 414 (2000).
26. A statistical model (*42*) was used to determine the standard errors of the trends in Table 1. An estimate of the trend (ω) for each time series was determined using a least-squares linear fit. The residual time series, N_t, is defined as the residual time series after removal of the mean, the annual cycle, and the linear trend from the original time series. If we define the variance of N_t as $\sigma^2_N = \mathrm{Var}(N_t)$, then the standard deviation of the trend can be approximated using equation 2 of (*42*) as $\sigma_\omega \approx \sigma_N/n^{3/2}[(1+\phi)/(1-\phi)]^{1/2}$, where the lag-1 autocorrelation is defined as $\phi = \mathrm{Corr}(N_t, N_{t-1})$ and n is the number of years in the monthly mean time series. Table 1 provides $\omega \pm 2\sigma_\omega$ for each time series. A trend may be considered to meet the 95% confidence level when $|\omega| > 2\sigma_\omega$.
27. W. Elliott, D. Gaffen, *Bull. Am. Meteorol. Soc.* **72**, 1507 (1991).
28. B. Soden, F. Bretherton, *J. Geophys. Res.* **98**, 16669 (1993).
29. We use an updated set of clear-sky radiances from HIRS as described in (*32*). Although there could be deficiencies in the cloud-screening methodology that might bias the observed T12, the most recent analysis of cirrus clouds from HIRS, using a method specifically designed to detect thin cirrus, indicates no discernible trend in high-level cloud cover over the period of record (*43*).
30. To avoid uncertainties associated with the inversion of satellite-measured radiances into geophysical quantities, we input the GCM profiles of temperature and water vapor mixing ratio into a narrow-band radiative transfer model to simulate the T12 that the HIRS instrument would have observed under those conditions. The radiative transfer model used here is the HIRS Fast Forward Program (HFFP) (*44*).
31. J. Bates, X. Wu, D. Jackson, *J. Clim.* **9**, 427 (1996).
32. J. Bates, D. Jackson, *Geophys. Res. Lett.* **28**, 1695 (2001).
33. B. Soden, R. Fu, *J. Clim.* **8**, 2333 (1995).
34. A. Geer, J. Harries, H. Brindley, *J. Clim.* **12**, 1940 (1999).
35. R. Allan, M. Ringer, A. Slingo, *Q. J. R. Meteorol. Soc.* **129**, 3371 (2003).
36. M. McCarthy, R. Toumi, *J. Clim.* **17**, 3181 (2004).
37. J. Christy, R. Spencer, W. Braswell, *J. Atmos. Oceanic Technol.* **17**, 1153 (2000).
38. C. Mears, M. Schabel, F. Wentz, *J. Clim.* **16**, 3650 (2003).
39. C. A. Mears, F. J. Wentz, *Science* **309**, 1548 (2005); published online 11 August 2005 (10.1126/science.1114772).
40. B. D. Santer *et al.*, *Science* **309**, 1551 (2005); published online 11 August 2005 (10.1126/science.1114867).
41. Global Atmospheric Model Development Team, *J. Clim.* **17**, 461 (2004).
42. E. C. Weatherhead *et al.*, *J. Geophys. Res.* **103**, 17149 (1998).
43. D. Wylie, D. L. Jackson, W. P. Menzel, J. J. Bates, *J. Clim.* **18**, 3021 (2005).
44. B. Soden *et al.*, *Bull. Am. Meteorol. Soc.* **81**, 797 (2000).

45. Supported in part by the NOAA Office of Global Programs.

Supporting Online Material

www.sciencemag.org/cgi/content/full/1115602/DC1
SOM Text
Fig. S1
References

1 June 2005; accepted 29 September 2005
Published online 6 October 2005;
10.1126/science.1115602
Include this information when citing this paper.

Synthesis of a Stable Compound with Fivefold Bonding Between Two Chromium(I) Centers

Tailuan Nguyen,[1] Andrew D. Sutton,[1] Marcin Brynda,[1] James C. Fettinger,[1] Gary J. Long,[2] Philip P. Power[1]*

Although in principle transition metals can form bonds with six shared electron pairs, only quadruply bonded compounds can be isolated as stable species at room temperature. Here we show that the reduction of $\{Cr(\mu\text{-}Cl)Ar'\}_2$ [where Ar′ indicates C_6H_3-2,6(C_6H_3-2,6-Pr^i_2)$_2$ and Pr^i indicates isopropyl] with a slight excess of potassium graphite has produced a stable compound with fivefold chromium-chromium (Cr–Cr) bonding. The very air- and moisture-sensitive dark red crystals of Ar′CrCrAr′ were isolated with greater than 40% yield. X-ray diffraction revealed a Cr–Cr bond length of 1.8351(4) angstroms (where the number in parentheses indicates the standard deviation) and a planar trans-bent core geometry. These data, the structure's temperature-independent paramagnetism, and computational studies support the sharing of five electron pairs in five bonding molecular orbitals between two $3d^5$ chromium(I) ions.

A quadruple bond between metal centers consisting of σ, 2π, and δ orbital overlaps was shown to be present in salts containing the $[Re_2Cl_8]^{2-}$ ion in 1964 (*1*). Since then, a rich chemistry has developed around this class of transition-metal compounds (*2*), whose bond order exceeds the previously known limit of three for compounds of the p-block elements. Beginning in the mid-1970s, theoretical and spectroscopic investigations of diatomic transition-metal species M_2 (where M is either Cr or Mo) trapped in inert matrices at low temperatures indicated that sextuple bonds consisting of 2σ, 2π, and 2δ overlaps (derived from valence s and d atomic orbitals) could exist between these metals (*3–14*). However, such molecules have no stable existence at room temperature and so cannot be isolated for bulk manipulation.

If ligands are used to stabilize multiply bonded metal centers, their binding reduces the

[1]Department of Chemistry, One Shields Avenue, University of California, Davis, CA 95616, USA. [2]Department of Chemistry, University of Missouri-Rolla, Rolla, MO 65409–0010, USA.

*To whom correspondence should be addressed. E-mail: pppower@ucdavis.edu

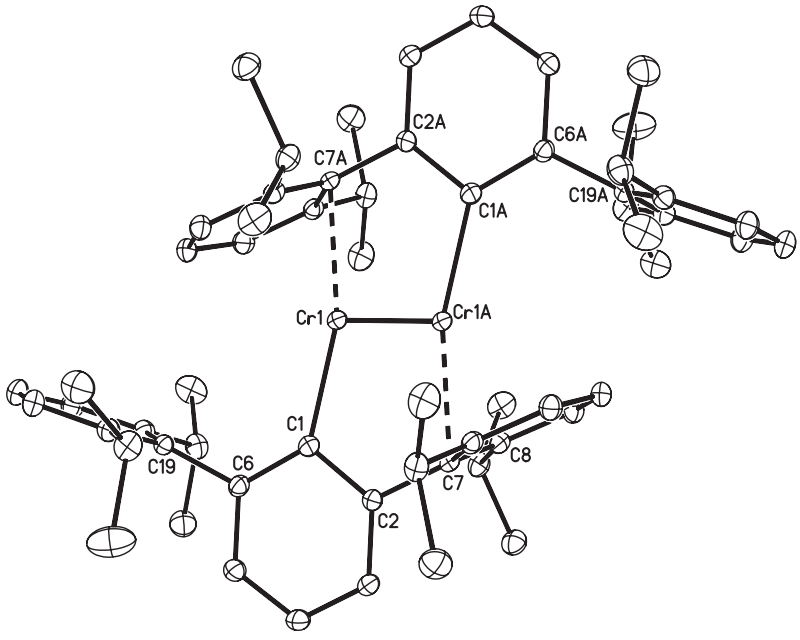

Fig. 1. Thermal ellipsoid (30%) drawing of Ar′CrCrAr′ (compound **1**). Hydrogen atoms are not shown. Selected bond distances and angles ° are as follows: Cr(1)–Cr(1A), 1.8351(4) Å; Cr(1)–C(1), 2.131(1) Å; Cr(1)–C(7A), 2.2943(9) Å; Cr(1)–C(8A), 2.479(1) Å; Cr(1)–Cr(12A), 2.414(1) Å; C(1)–C(2), 1.421(1) Å; C(1)–C(6), 1.423(2) Å; C(7)–C(8), 1.421(1) Å; C(7)–C(12), 1.424(1) Å; Cr(1A)–Cr(1)–C(1), 108.78(3)°; Cr(1A)–Cr(1)–C(7A), 94.13(3)°; C(1)–Cr(1)–C(7A), 163.00(4)°; Cr(1)–C(1)–C(2), 114.34(7)°; Cr(1)–C(1)–C(6), 131.74(7)°; and C(2)–C(1)–C(6), 113.91(9)°.

number of valence orbitals available to form metal-metal bonds. Thus, the number of ligands must be minimized, and the number of metal valence electrons that fill bonding orbitals must be maximized in order to achieve the highest bond order possible in an isolable compound. Moreover, the ligands must be sufficiently bulky to inhibit intermolecular reactions that yield clusters or polymers with lower bond orders. We have shown (*15*) that the sterically encumbering monovalent terphenyl ligand C_6H_3-2,6(C_6H_3-2,6-Pr^i_2)$_2$ (hereafter designated Ar′), where Pr^i is isopropyl, and related derivatives can stabilize many compounds with low coordination numbers or unusual bonding (*16*, *17*). We now show that this ligand allows room-temperature isolation of the Ar′CrCrAr′ chromium dimer to occur. The structural, spectroscopic, and magnetic properties of this compound are consistent with a quintuple Cr–Cr bond formed by a fivefold overlap between the metal d orbitals (*18*).

The compound Ar′CrCrAr′ (compound **1**) was isolated as dark red crystals from the reduction of {Ar′Cr(μ-Cl)}$_2$ with KC_8 (*19*). The crystals are thermally robust and decompose slowly above 200°C, but they are spontaneously flammable when exposed to air. X-ray crystallography of **1** (Fig. 1) (*20*) showed a structure characterized by a center of symmetry at the midpoint of the very short [1.8351(4) Å, where the number in parentheses indicates SD] Cr–Cr bond. Each Cr is bonded to the ipso carbon atom [distance Cr(1)–C(1) = 2.131(1) Å] of an Ar′ substituent. There is also a weaker interaction between each Cr ion [Cr(1)–C(7A) = 2.2943(9) Å] and the ipso carbon [C(7) or C(7A)] of a flanking ring of the terphenyl group attached to the other Cr. The core atoms, C(1)Cr(1)Cr(1A)C(1A), are coplanar, but they have a trans-bent structure with C_{2h} local symmetry and a bending Cr(1A)Cr(1)C(1) angle of 102.78(3)°. Magnetic measurements revealed a temperature-independent paramagnetism of 0.000112(5) electromagnetic units (emu) per mol of Cr (*21*). The electronic absorption spectrum of **1** displays strong absorptions below 250 nm and a broad absorption at 488 nm, with an intensity (ε) of 3200 mol^{-1} L cm^{-1}.

The metal-metal bonding in compound **1** arises from the interaction of two Cr(I) centers with d^5 electron configurations. In a simplified molecular-orbital overlap diagram with the assumption of local C_{2h} symmetry, five metal-metal bonding molecular orbitals can be visualized (Fig. 2) (*22*, *23*). Also, two further metal-ligand orbital combinations, bonding and antibonding with respect to the metal-metal bond, are present. The bonding is actually more complex, because mixing of the orbitals with the same symmetry (i.e., 4s and $3d_{z^2}$ or $3d_{x^2-y^2}$) can occur. Nonetheless, σ ($d_{z^2} - d_{z^2}$, A_g), 2π ($d_{yz} - d_{yz}$, $d_{xz} - d_{xz}$, A_u, B_u), and 2δ ($d_{x^2-y^2} - d_{x^2-y^2}$, $d_{xy} - d_{xy}$, A_g, B_g) Cr–Cr overlaps, in which electrons from each metal become paired to fill the five bonding orbitals, are possible (*23*).

This fivefold Cr–Cr interaction is supported by structural and magnetic data. The Cr–Cr distance is extremely short and is very close to the 1.828(2) Å bond found in the Cr(II) dimer, $Cr_2\{C_6H_3$-2-OMe-5-Me$\}_4$, which has the shortest reported metal-metal bond distance (*24*). In this Cr(II) compound and related species, the chelating nature of the ligand plays a key role in pushing the Cr centers close together, and it could be argued that the Ar′ ligand acts similarly in **1** through the secondary Cr—C interactions. However, we have also synthesized the related Ar′FeFeAr′ and Ar′CoCoAr′ dimers, which are structurally similar to **1** but have much longer Fe–Fe and Co–Co distances, ~2.53 and 2.80 Å, respectively. Thus, the Ar′ ligand can accommodate M-M separations that vary by almost 1 Å. For this reason, the bridging shown by the Ar′ ligand in **1** is unlikely to be the cause of the short metal-metal distance. In other words, the very short Cr–Cr bond in **1** is mainly due to the interaction of the d^5 Cr centers, rather than a constraining ligand geometry (*25*).

The temperature-independent weak paramagnetism of **1** is also consistent with strongly coupled d^5-d^5 bonding electrons. Temperature-independent paramagnetism has been observed for several other M-M–bonded transition-metal complexes (*26*–*29*). Nonetheless, the possibility that the Cr–Cr multiple bond may be a combination of covalent bonding with antiferromagnetic coupling, which was recently calculated for the Cr_2 dimer (*14*), should not be dismissed. The distinction between antiferromagnetic coupling and what constitutes a bond is not clearly defined; therefore, it would be of great interest to determine the contribution of the antiferromagnetic exchange coupling to the overall Cr–Cr bond energy. This exchange coupling is so strong in **1** between 2 and 300 K that, unfortunately, there is no increase in the susceptibility as the $S > 0$ states are populated; i.e., $-2J$, the antiferromagnetic exchange coupling, is so negative that only the $S = 0$ ground state is effectively populated at these temperatures. As a consequence, the susceptibility never begins to increase with increasing temperature, and it is difficult to determine $-2J$. The unpopulated $S > 0$ excited states yield a second-order Zeeman contribution of 0.00112(5) emu/mol Cr to the molar magnetic susceptibility. This is the so-called "temperature-independent paramagnetism" (TIP), a contribution which must be added to the essentially zero contribution of the $S = 0$ ground state.

Further insight on the bonding in **1** may be obtained from computational data. However, calculations on multiply bonded transition-metal species have often been difficult because of electron correlation problems (*30*, *31*). Nonetheless, recent studies (*8*, *32*, *33*) have suggested that density functional theory (DFT) methods can compete successfully with high-level ab initio calculations. Both the trans-bent geometry and the quintuple-bond formulation are predicted by the simple, Lewis-like electron-

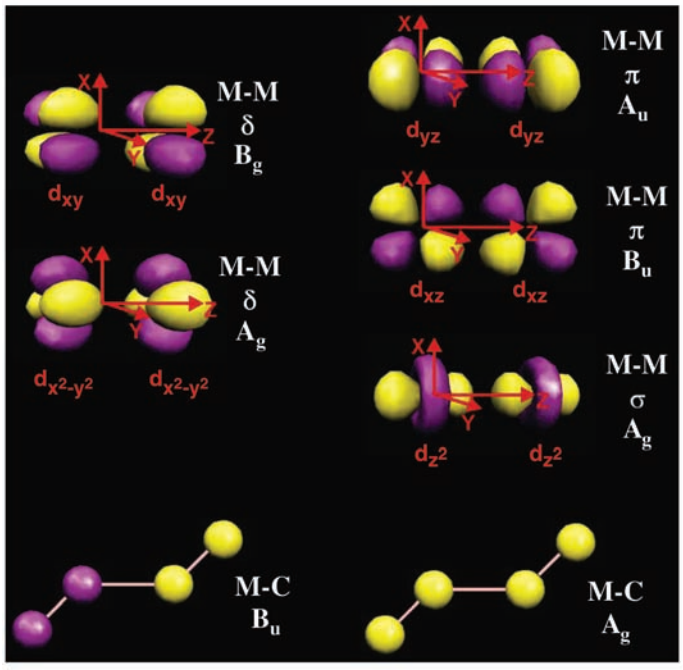

Fig. 2. (**Left**) Schematic drawing of simplified molecular orbital overlaps for M-M and M-C bonding.

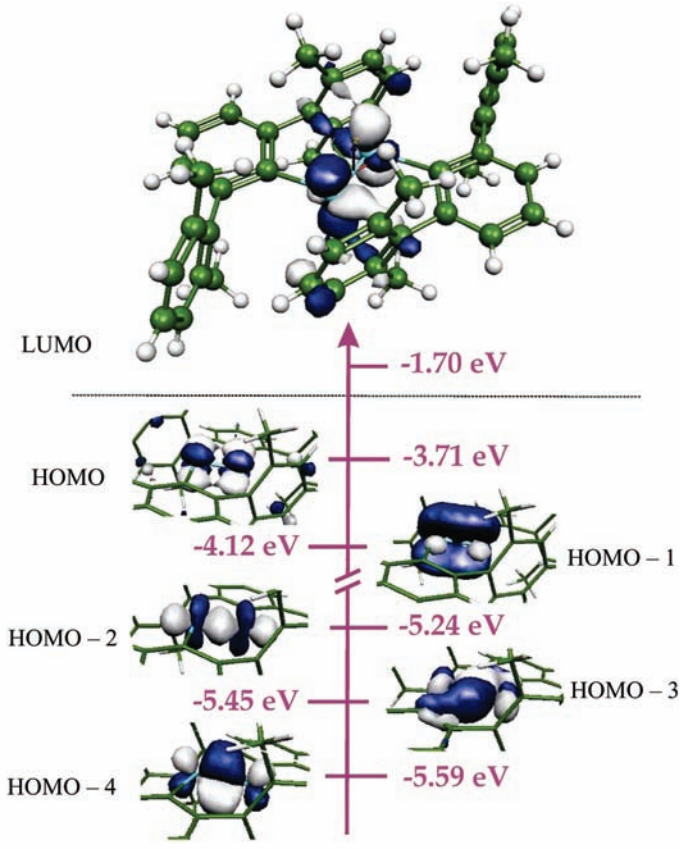

Fig. 3. (**Right**) Electron density surfaces and energies for the Cr–Cr bonding orbitals in Ar′CrCrAr′ (*36*).

pair sharing scheme of Landis and Weinhold for transition-metal complexes (*34*, *35*). We carried out restricted DFT calculations (*36*) using hybrid and pure functionals to further analyze the Cr–Cr interaction. These theoretical approaches (*37*) yielded very similar results. Molecular orbitals were generated from single-point calculations by using the atomic coordinates provided by the x-ray structure. The metal-metal orbital surfaces (Fig. 3) support the view that there are five orbital interactions between the Cr(I) ions. The symmetries of the highest occupied molecular orbital (HOMO) and HOMO – 1, which differ in energy by 0.41 eV, correspond to δ bonds. The HOMO – 2 corresponds to Cr–Cr σ bonding and lies at ~1.08 eV lower energy than HOMO – 1. HOMO – 3 and HOMO – 4 correspond to Cr–Cr π bonds and lie slightly (~0.21 to 0.35 eV) below the σ-bonding level.

The calculated HOMO–lowest unoccupied molecular orbital (LUMO) energy gap (2.01 eV, 46.35 kcal mol^{-1}), which may correspond to a δ-δ* transition, is at a somewhat lower energy than the 58.59 kcal mol^{-1} calculated from the 488-nm absorption maximum in the electronic spectrum. This discrepancy has precedent in $\sigma^2\pi^4\delta^2$ quadruply bonded M-M species, for which the experimental δ-δ* transition energies are usually higher than those calculated (*2*). Moreover, the putative δ-δ* transition lies at the higher energy end of the ~450 to 1600-nm range observed for quadruply bonded compounds (*2*), which suggests that the δ bonds in **1** are as strong as those observed in the quadruply bonded compounds.

References and Notes

1. F. A. Cotton *et al.*, *Science* **145**, 1305 (1964).
2. F. A. Cotton, L. A. Murillo, R. A. Walton, *Multiple Bonds Between Metal Atoms* (Springer, Berlin, ed. 3, 2005).
3. E. P. Kündig, M. Moskovits, G. A. Ozin, *Nature* **254**, 503 (1975).
4. W. Klotzbücher, G. A. Ozin, *Inorg. Chem.* **16**, 984 (1977).
5. J. G. Norman Jr., H. J. Kolari, H. B. Gray, W. C. Trogler, *Inorg. Chem.* **16**, 987 (1977).
6. B. E. Bursten, F. A. Cotton, M. B. Hall, *J. Am. Chem. Soc.* **102**, 6349 (1980).
7. M. D. Morse, *Chem. Rev.* **86**, 1049 (1986).
8. C. J. Barden, J. C. Rienstra-Kiracofe, H. F. Schaefer III, *J. Chem. Phys.* **113**, 690 (2000).
9. S. Yanagisawa, T. Tsuneda, K. Hirao, *J. Chem. Phys.* **112**, 545 (2000).
10. E. A. Boudreaux, E. Baxter, *Int. J. Quantum Chem.* **85**, 509 (2001).
11. G. L. Gutsev, C. W. Bauschlicher Jr., *J. Phys. Chem. A* **107**, 4755 (2003).
12. B. O. Roos, *Collect. Czech. Chem. Commun.* **68**, 265 (2003).
13. J. L. Jules, J. R. Lombardi, *J. Phys. Chem. A* **107**, 1268 (2003).
14. E. A. Boudreaux, E. Baxter, *Int. J. Quantum Chem.* **100**, 1170 (2004).
15. B. Schiemenz, P. P. Power, *Angew. Chem. Int. Ed. Engl.* **35**, 2150 (1996).
16. B. Twamley, S. T. Haubrich, P. P. Power, *Adv. Organomet. Chem.* **44**, 1 (1999).
17. J. A. C. Clyburne, N. McMullen, *Coord. Chem. Rev.* **210**, 73 (2000).
18. The description "quintuple bond" is intended to indicate that five electron pairs play a role in holding the metal atoms together. It does not imply that the bond order is five or that the bonding is very strong, because the ground state of the molecule necessarily involves mixing of other higher-energy configurations with less bonding character. This gives lower, usually noninteger, bond orders. Further discussion of bond order in transition metal complexes can be found in (*2*).
19. All manipulations were carried out under anaerobic and anhydrous conditions. With rapid stirring, a solution of $\{Cr(\mu\text{-}Cl)Ar'\}_2$ [1.94 g, 2 mmol, synthesized in 70% yield from a [1:1] tetrahydrofuran (THF, 30 mL) solution of $CrCl_2(THF)_2$ and LiAr′ (*15*)] was added dropwise to a suspension of freshly prepared KC_8 (0.68 g, 5.0 mmol) in THF (15 mL) being cooled with an ice bath. The resulting dark suspension in a red solution was stirred for 16 hours to ensure complete reduction. The volatile materials were removed under reduced pressure, and a toluene (25 mL) extract of the solid was filtered, reduced to ~15 mL, and left for 2 days at 7°C, after which 0.74 g (41% yield) could be isolated as dark red, x-ray–quality crystals with decomposition > 200°C. Ultraviolet (UV)/visible (vis) [hexanes, given as maximum wavelength (λ_{max}) in nm and, in parenthesis, ε in mol^{-1} L cm^{-1})] is 488 (3200). Infrared (nujol) frequency ν = 1261s, 1092s, 1020s, 867w, 799s, 493w cm^{-1}, where s is strong and w is weak. Magnetic susceptibility χ_M = 0.00112 emu/mol Cr at 2 to 300 K combustion analysis (We found the following: C, 80.72%; H, 8.01%. Calculation for $C_{60}H_{74}Cr_2$ gave: C, 80.14%; H, 8.29%).
20. Crystal data for **1**• $2C_7H_8$ were obtained at 90(2) K with use of a Bruker SMART 1000 diffractometer and MoK_α radiation (λ = 0.71073 Å). The crystal data are as follows: *a* = 9.9982(15) Å, *b* = 10.8869(16) Å, *c* = 14.410(2) Å, α = 88.641(2)°, β = 82.242(3)°, γ = 76.129(2)°, triclinic, *Z* = 1, R_1 for 7931 [data intensity $I > 2\sigma(I)$] data = 0.0320, wR_2 (all data) = 0.0939.
21. For magnetic measurements, the samples were sealed under N_2 in 2-mm quartz tubing. The sample magnetization was measured with use of a Quantum Design MPMSXL7 superconducting quantum interference device (SQUID) magnetometer. For each measurement, the sample was zero-field cooled to 5 K, and the

magnetization was measured as a function of field to 2 T. The field was then reduced to 1 T, and the magnetization of the sample was measured in 5-K increments to 300 K. The observed susceptibility was corrected for the 0.000374–emu/mol Cr diamagnetic contribution to the susceptibility, a correction which was obtained from tables of Pascal constants. The extreme air sensitivity of **1** results in 2 to 6% contamination of all samples examined so far with paramagnetic impurities that involve Cr in higher oxidation states. It is also possible that the paramagnetic impurities could arise from incomplete or over reduction of $\{Cr(\mu\text{-}Cl)Ar'\}_2$. A plot of the molar magnetic susceptibility versus temperature for **1** is given in (*37*).
22. A different type of quintuple bond, which consists of three electron-pair bonds and four one-electron bonds, has been calculated to exist in U_2 molecules (*23*).
23. L. Gagliardi, B. O. Roos, *Nature* **433**, 848 (2005).
24. F. A. Cotton, S. A. Koch, M. Millar, *Inorg. Chem.* **17**, 2084 (1978).
25. The secondary Cr–C interaction involving a flanking aryl ring is due in part to the electron deficiency of the Cr center (12 electrons) and the electropositive character of the metal. It is also probable that the secondary Cr–C interaction lengthens the Cr–Cr bond because the "extra" Cr–C interaction competes for the chromium orbitals, thereby weakening the Cr–Cr bonding. Furthermore, all the Cr–C interactions occur in one plane so that the Ar′ ligands are eclipsed, which increases steric congestion and causes the Cr–Cr bond to lengthen. The existence of the eclipsed structure in **1** and its absence in the corresponding Ar′FeFeAr′ and Ar′CoCoAr′ species are consistent with the presence of δ bonding. The possibility that **1** featured bonds between chromium and hydrogen (i.e., an Ar′-substituted Cr(II) hydride derivative) was also entertained. No evidence for a Cr-H moiety could be observed in the infrared (IR) or ^{1}H nuclear magnetic resonance (NMR) spectrum of **1**. X-ray data and computational studies (*35*) also supplied no indication of the presence of the hydrogens near Cr.
26. P. D. Ford, L. F. Larkworthy, D. C. Povey, A. J. Roberts, *Polyhedron* **2**, 1317 (1983).
27. C. J. Bilgrien, R. S. Drago, C. J. O'Connor, N. Wong, *Inorg. Chem.* **27**, 1410 (1988).
28. F. A. Cotton, H. Chen, L. M. Daniels, X. Feng, *J. Am. Chem. Soc.* **114**, 8980 (1992).
29. R. Clerac *et al.*, *Inorg. Chem.* **29**, 2581 (2000).
30. M. B. Hall, *Polyhedron* **6**, 679 (1987).
31. D. R. Salahub, in *Ab Initio Methods in Quantum Chemistry, Part 2, Advances in Chemical Physics, Vol. 69*, K. P. Lawley, Ed. (Wiley, New York, 1987), pp. 447–518.
32. Recent computational studies of dimetal species using several different functionals have shown that the calculated M-M distances can vary by as much as 0.24 Å (*33*).
33. N. E. Schultz, Y. Zhao, D. G. Truhlar, *J. Phys. Chem. A* **109**, 4388 (2005).
34. F. Weinhold, C. R. Landis, *Chem. Ed. Res. Pract. Eur.* **2**, 91 (2001).
35. F. Weinhold, C. R. Landis, *Valency and Bonding* (Cambridge Univ. Press, Cambridge, 2005), p. 355.
36. The electronic structure of **1** was calculated using DFT at restricted level (B3LYP/6-31*). Calculations were also performed using pure BP86 and BLYP functionals, which yielded very similar results. Additional DFT calculations carried out on **1** using the unrestricted Kohn-Sham broken symmetry (UKS-BS) approach yielded a wave function corresponding to a singlet diradical ground state with antiferromagnetic coupling between the two electrons that occupy the HOMO orbital. Other details of the DFT calculations are reported in (*35*).
37. Materials and methods are available as supporting material on *Science* Online.
38. We are grateful to the donors of the Petroleum Research Fund administered by the American Chemical Society and NSF for financial support of this work. In addition, we thank P. Klavins and L. D. Pham of the Department of Physics at the University of California, Davis, for recording the magnetic data, and C. R. Landis and E. Sinn for useful discussions. Metrical data for compound **1** are freely available from the Cambridge Crystallographic Database Centre (CCDC – 276888).

Supporting Online Material
www.sciencemag.org/cgi/content/full/1116789/DC1
Materials and Methods
Figs. S1 to S3
Tables S1 to S16
References and Notes

30 June 2005; accepted 8 September 2005
Published online 22 September 2005;
10.1126/science.1116789
Include this information when citing this paper.

A Direct Role for Dual Oxidase in *Drosophila* Gut Immunity

Eun-Mi Ha,[1] Chun-Taek Oh,[2] Yun Soo Bae,[1] Won-Jae Lee[1,2]*

Because the mucosal epithelia are in constant contact with large numbers of microorganisms, these surfaces must be armed with efficient microbial control systems. Here, we show that the *Drosophila* nicotinamide adenine dinucleotide phosphate (NADPH) oxidase enzyme, dual oxidase (dDuox), is indispensable for gut antimicrobial activities. Adult flies in which *dDuox* expression is silenced showed a marked increase in mortality rate even after a minor infection through ingestion of microbe-contaminated food. This could be restored by the specific reintroduction of dDuox, demonstrating that this oxidase generates a unique epithelial oxidative burst that limits microbial proliferation in the gut. Thus, oxidant-mediated antimicrobial responses are not restricted to the phagocytes, but rather are used more broadly, including in mucosal barrier epithelia.

The innate immune system provides an essential means of host defense in eukaryotes against a broad spectrum of microorgansims (*1*), and the production of microbicidal reactive oxygen species (ROS) is a key feature of this protective response (*2*–*6*). To date, most studies have focused on the molecular mechanism of respiratory burst in the professional phagocytes in response to microbial infection (*2*–*6*). In contrast, the oxidant-dependent antimicrobial properties in mucosal epithelia, which are in permanent contact with the microbial realm, remain largely unknown. In *Drosophila*, the nuclear factor κB (NF-κB) pathways are critical during systemic infection (*7*–*11*) but appear to be less than crucial for host survival after epithelial infection (*12*). Natural gut infection has been associated with the rapid synthesis of ROS (*12*), and the dynamic cycle of ROS generation and elimination appears to be vital in *Drosophila*, because flies that lack ROS-removal capacity have an increased mortality (*12*). Such observations suggest an imortant role for ROS generation in controlling epithelial infection.

To directly examine if the epithelial oxidative burst system is required for host survival, we tested the potential superoxide-producing activity of intestinal epithelia in vitro (*13*). A basal level of superoxide generation was maintained in the membrane fraction of dissected intestines, and this increased markedly in the presence of calcium in a dose-dependent manner (Fig. 1A). Treatment with EGTA, or diphenylene iodonium (DPI), which is a flavoprotein inhibitor that also inhibits the nicotinamide adenine dinucleotide phosphate (NADPH) oxidase–dependent oxidative burst, completely blocked calcium-activated intestinal superoxide-producing activity (Fig. 1A). In humans, phagocytic cells generate the ROS precursor, superoxide, via the phagocytic oxidase (phox) complex (*2*, *5*). Recently, the human genome has been shown to contain several NADPH oxidase family members [currently designated the Nox 1-5 and dual oxidase (Duox) 1-2], each of which is homologous to the phox catalytic subunit, gp91^{phox}/Nox2 (*14*, *15*). The Duox family can be distinguished from the Nox family based on the presence of an N-terminal extracellular peroxidase-homology domain (PHD) in addition to the gp91^{phox}-like oxidase domain (*14*, *15*). The Nox/Duox family of enzymes are expressed in a variety of nonphagocytic cells, suggesting that they require oxidase functions similar to those of gp91^{phox}/Nox2 (*16*–*18*). Recently, Duox has been shown to be expressed in the barrier epithelia, including epithelial cells of mucosal surfaces of colon, rectum, salivary gland ducts, and bronchi (*18*–*20*), and it has been suggested that Duox may provide an epithelial ROS source in host defense (*18*–*20*). To determine the in vivo role of *Drosophila* Nox and Duox homologs (dNox and dDuox, respectively) (fig. S1) with regard to epithelial immunity, we generated a set of loss-of-function trans-

[1]Division of Molecular Life Science and Center for Cell Signaling Research, Ewha Woman's University, Seoul 120-750, South Korea. [2]Laboratory of Innate Immunity, Institut Pasteur Korea, Seoul 136-791, South Korea.

*To whom correspondence should be addressed. E-mail: lwj@ewha.ac.kr